Title

Stabilizing Aqueous Three-Dimensional Printed Constructs Using Chitosan-Cellulose Nanocrystal Assemblies

Journal

ACS Applied Materials & Interfaces, 12(49)

ISSN

1944-8244

Authors

Lin, Dandan

Liu, Tan

Yuan, Qingqing

et al.

Publication Date

2020-12-09

DOI

10.1021/acsami.0c16602

Peer reviewed

Conductive Thin Films Over Large Areas by Supramolecular Self-Assembly

Pei-Yang Gu,[1,2] Yufeng Jiang,[2,3] Zachary Fink,[4] Ganhua Xie,[2] Qin Hu,[2] Paul Y. Kim,[2] Qing-Feng Xu,[1] Jian-Mei Lu,[1] and Thomas P. Russell[2,4,5]**

[1]College of Chemistry, Chemical Engineering and Materials Science, Collaborative Innovation, Center of Suzhou Nano Science and Technology, Soochow University, Suzhou, 215123, P. R. China.

[2]Materials Sciences Division, Lawrence Berkeley National Laboratory, 1 Cyclotron Road, Berkeley, CA 94720, USA

[3]Applied Science and Technology, University of California, Berkeley, 210 Hearst Memorial Mining Building, Berkeley, CA 94720, USA

[4]Polymer Science and Engineering Department, University of Massachusetts, Amherst, MA 01003, USA

[5]Beijing Advanced Innovation Center for Soft Matter Science and Engineering, Beijing University of Chemical Technology, Beijing 100029, P. R. China.

KEYWORDS: block copolymers, supramolecular self-assembly, conductive thin films, porphyin, *in situ* GISAXS

ABSTRACT: We report a 'one step' method for preparing conductive thin films with cylindrical microdomains oriented normal to the surface over large areas using the supramolecular assembly of poly(styrene-*block*-4-vinylpyridine) (PS-*b*-P4VP) and 5,10,15,20-tetrakis(4-hydroxyphenyl)-21*H*,23*H*-porphine (HOTPP). The HOTPP interacts with the P4VP block by a hydrogen bonding between the hydroxyl group of HOTPP and pyridine ring of PS-*b*-P4VP, forming cylindrical P4VP(HOTPP) domains having an average diameter of ~17 nm in a PS matrix. Dynamic light scattering, contact angle, and *in situ* grazing incidence small-angle X-ray scattering analyses show a morphological transition from spherical micelles in solution to cylindrical microdomains oriented normal to the substrate surface during the drying process. From the dependence of current on voltage, an average current of ~ 4.0 nA is found to pass through a single microdomain, pointing to a promising route for organic semiconductor device applications.

The self-assembly of block copolymers (BCPs) has generated widespread attention in the areas of nanoscience and nanotechnology due to their formation of periodic arrays of nanoscopic domains that serve as scaffolds and templates for the fabrication of inorganic nanomaterials.[1-7] BCPs microphase separate into spherical, cylindrical, lamellar and gyroid microdomains, depending on the volume fraction and rigidity of the components and segmental interactions, while the size of the microdomains is dictated by the molecular weight.[8-11] Absent an external field, at equilibrium, the orientation of the microdomains is dictated by the interactions of the blocks with the substrate, surface energies of the blocks, segmental interactions and commensurability of the natural period of the copolymer and the film thickness.[12-14] However, processes, like solvent evaporation, where interfacial interactions can be mediated by the presence of the solvent and where there is a gradient in the field normal to the surface, i.e. solvent can evaporate only through the surface producing gradient in the solvent concentration, can be used to kinetically trap a specific orientation of the microdomains.[15-17] The orientation of the cylindrical microdomains normal to the film surface is of particular interest for fabricating high performance organic semiconductor devices such as organic resistance memory (ORM) device. If the microdomains oriented normal to the film surface, and the microdomains are semi-conductive, then thin films of BCPs could find use as, for example, active layers in ORM devices.

Low-molecular-weight additives that associate with one of the blocks of a BCP by noncovalent interactions afford a simple strategy to introduce new functionality and provide a simple route to fine-tune the morphology by solvent and/or thermal annealing.[18-22] These annealing processes, though, are energy intensive, environmentally unfriendly, and make

processing more complex, limiting the fabrication of large-scale films.[23-25] Ideally, the additive would serve to significantly enhance the microphase separation and mediate interfacial interaction so as to promote the orientation of the microdomains normal to the surface of the film, thereby eliminating post-processing steps.

Herein, a functional small molecule, 5,10,15,20-tetrakis(4-hydroxyphenyl)-21*H*,23*H*-porphine (HOTPP), that associates, by a hydrogen bonding, to the vinylpyridine groups of poly(styrene-*block*-4-vinylpyridine) (PS-*b*-P4VP, 19000-*b*-5000 g mol^{-1}), is used to tune the thin film morphologies by varying the ratio between HOTPP and vinylpyridine groups, as shown in Scheme 1 and Table 1. HOTPP was selected as the low-molecular-weight additive for two

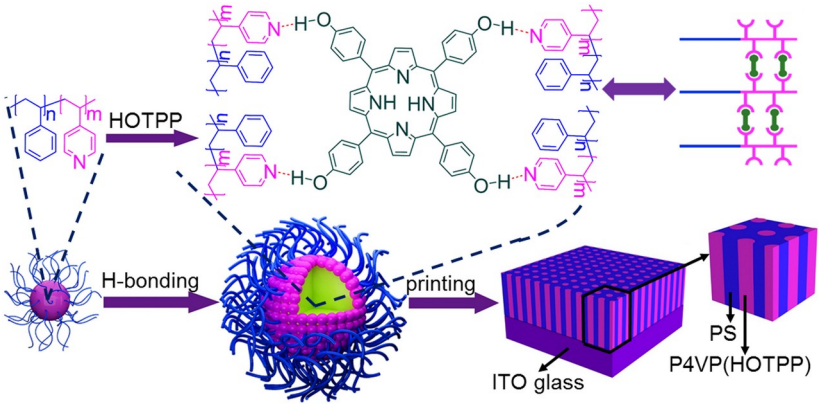

Scheme 1. Scheme of the fabrication thin film approach based on the supramolecular assembly.

reasons. First, each HOTPP contains four hydroxyl moeities that can hydrogen bond to the pyridine groups in the P4VP blocks, leading to significantly increase segmental interaction parameter and, also, to a convenient means to crosslink the assemblies. Second, the 18 π-electrons of HOTPP are coplanar enabling a π -stacking that leads to excellent electronic properties.[26, 27] Proton nuclear magnetic resonance (^{1}H NMR) and Fourier transform infrared

(FTIR) spectroscopies evidence the formation of hydrogen bonding between the pyridine groups on P4VP block and hydroxyl groups on HOTPP. Atomic force microscope (AFM) and *in situ* grazing incidence small-angle X-ray scattering (GISAXS) enabled the investigation of the evolution of the morphology, specifically a transition from spherical micelles in solution to cylindrical microdomains oriented normal to the substrate as the solvent evaporated. The electronic properties of the supramolecular thin films were also investigated.

RESULTS AND DISCUSSION

We construct supramolecules (SMs) by attaching HOTPP to PS-*b*-P4VP *via* a hydrogen bonding between hydroxyl moeities on HOTPP and the pyridine groups on P4VP block. The

Table 1. Characteristics of PS-b-P4VP(HOTPP)

Sample	$f_{P4VP(HOTPP)}$[a](%)	4VP/OH[b]	D[c](nm)	D[d](nm)
SM1	20.83	1:0	12.00	-
SM2	22.39	16.81/1	16.49	-
SM3	23.88	8.40/1	16.79	18
SM4	25.31	5.60/1	16.84	18
SM5	26.70	4.20/1	17.25	18
SM6	34.03	1.68/1	19.36	18
SM7	36.16	1.40/1	21.13	20
SM8	40.02	1.05/1	19.14	19
SM9	43.39	0.84/1	19.13	19
SM10	100	0/1	-	-

[a]Weight fraction between PS-b-P4VP(HOTPP).

[b]Stoichiometric (molar) ratio of pyridine to hydroxy groups.

[c]The hydrodynamic radius of micelle of PS-b-P4VP(HOTPP) was measured by dynamic light scattering.

[d]The microdomain spacing was measured by small angle X-ray scattering.

resultant SMs are identified as SM1to SM10 where the specific details are provided in Table 1 and the supporting information.

A high volume fraction of P4VP(HOTPP) ensures efficient charge carrier injection and transport. However, for highly crystalline organic molecules, such as HOTPP, at higher volume fractions of P4VP(HOTPP) there is a strong tendency for the molecules to aggregate, making it challenging to generate uniform films.[28, 29] Consequently, there is a delicate balance between the volume fraction of P4VP(HOTPP) and film uniformity, which is critical for the device performance. Figure 1 and Figure S1 show the AFM height images of spin-coated thins films

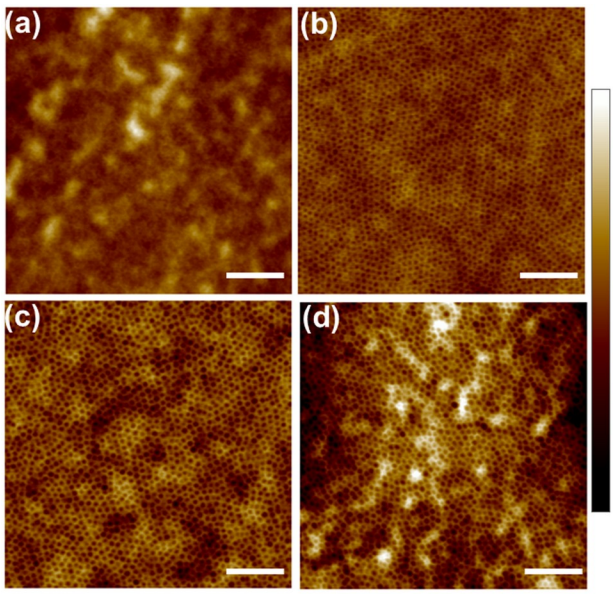

Figure 1. AFM height images of thin films spin coated from a toluene/THF (6:4, v:v) mixture solution absent any post treatment. (a) SM1, (b) SM5, (c) SM7, and (d) SM8. Scare bar: 200 nm and z scale: 10 nm.

absent post annealing treatments. The supramolecular thin films show different morphologies depending on the volume fractions of the components due to the intermolecular P4VP with HOTPP interactions. For low concentrations of HOTPP, the surface of the films are featureless,

with no strong evidence of either microphase separation or microdomains oriented normal to the films surface. However, by increasing the HOTPP to 27 % (Figure 1b) or higher, cylindrical microdomains oriented normal to the substrate are observed. At higher concentrations of HOTPP (above 40 %), aggregates of HOTPP (bright areas in the AFM images in Figure 1d and Figure S1h/1i) are seen, indicating a saturation of the interactions of the PS-*b*-P4VP, with the excess HOTPP forming aggregates. Consequently, SM7 represents the optimum balance with the highest volume fraction of P4VP(HOTPP) while maintaining film uniformity. UV-vis absorption and grazing incidence wide-angle X-ray scattering (GIWAXS) were consistent with the AFM results, as shown in Figure S3/S4. Pristine HOTPP shows a Soret band absorption at 427 nm and a broader Q-band absorption at 665 nm. At low HOTPP concentrations (e.g., SM2 and SM3), a Soret band absorption is evident at 433 nm which is red-shifted from the pristine HOTPP, indicating that the intermolecular interactions between HOTPP molecules decrease, since PS-*b*-P4VP can disperse HOTPP. By further increasing the concentration of HOTPP (e.g. SM5 and SM7), the wavelength of the Soret band does not change and Q-bands at 529, 565, 607, and 653 nm are observed, due to the increase in the absorption coefficient. At high HOTPP concentrations (e.g. SM8), a tail appears due to a light scattering effect, indicating that HOTPP can stack by π-π stacking which is further confirmed by GIWAXS results. Figure S4 shows the GIWAXS patterns of SM1, SM7-SM10. The thin film based on PS-*b*-P4VP shows a broad peak at 1.358 nm^{-1}. The shape and position have no obvious change with increasing the volume fraction of P4VP(HOTPP). However, for SM8, a new interference is observed at 1.542 nm^{-1} which corresponds to the pure HOTPP, suggesting that intermolecular interaction between HOTPP increases with increasing the volume fraction of P4VP(HOTPP).

^{1}H NMR and FT-IR spectroscopies provide evidence for hydrogen bonding between the pyridine groups on P4VP block and hydroxyl groups on HOTPP. Figure 2a shows the ^{1}H NMR analyses of pure polymer PS-*b*-P4VP, small molecule HOTPP, and SM7. In comparison to pure PS-b-P4VP, the peak arising from the P4VP block at 3-position is shifted from 8.43 to 9.00 ppm and that of the hydroxyl groups on HOTPP is shifted from 8.78 to 8.84 ppm, indicating interaction between the pyridine groups of the P4VP block and hydroxyl groups of the HOTPP.

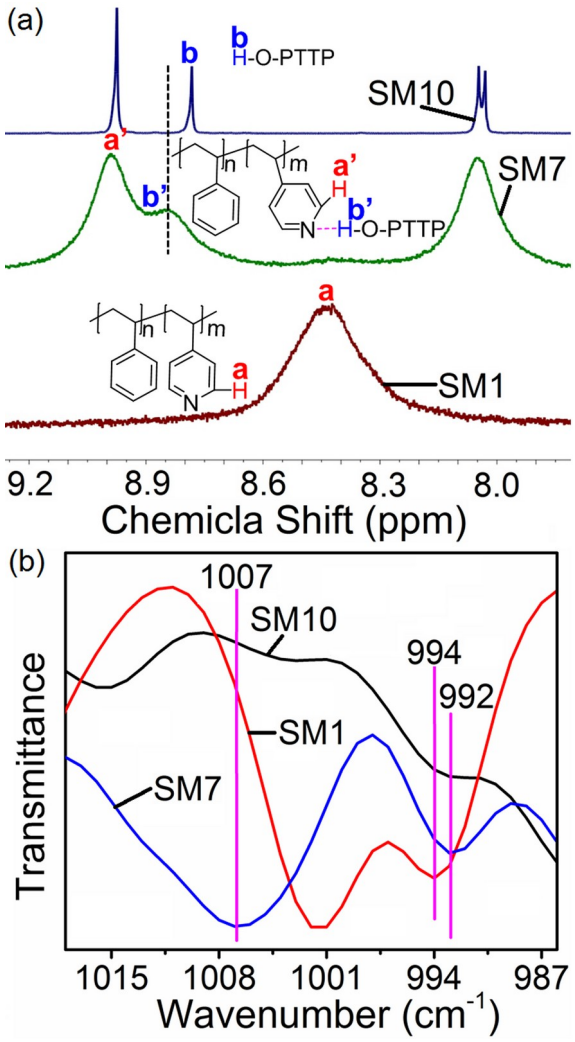

Figure 2. (a) ^{1}H NMR spectra of PS-*b*-P4VP (SM1), SM7, and HOTPP (SM10) in toluene-d_7/THF-d_4. (b) FT-IR spectra of SM1, SM7, and SM10.

Noting that the peak (8.43 ppm) arising from the P4VP block at 3-position and the peak (8.78) arising from the hydroxyl groups on the HOTPP almost vanishes for SM7, indicating that there is virtually no pure BCP PS-b-P4VP or free small molecule HOTPP in toluene-d7/THF-d4 solution. In comparison to pure HOTPP, the peaks arising from HOTPP in SM7 are significantly broadened, indicating that the small molecules, due to the hydrogen bonding, are no longer free and motions are severely retarded. The peaks arising from PS are essentially unchanged (Figure S6), as would be expected. Figure 2b compares FT-IR spectra in the 986-1018 cm^{-1} region for pure BCP PS-*b*-P4VP, small molecule HOTPP, and SM7. The absorption arising from free pyridine groups at 994 cm^{-1} which almost vanishes for SM7. However, a new absorption for SM7 is seen at 1007 cm^{-1} corresponding to the hydrogen-bonded pyridine. This result is very similar to that reported elsewhere for hydrogen bonds of pyridine groups on P4VP block with the hydroxyl groups of other small molecules.[30, 31] The ^{1}H NMR and FT-IR results indicate the interactions occur only between the pyridine groups of the P4VP block and the hydroxyl groups on the HOTPP.

Previous work has shown that PS-*b*-P4VP forms micelles in the toluene/THF (6:4, v:v) mixed solvents with the soluble PS block in the corona and the insoluble P4VP block in the core.[32] Table 1 shows that the hydrodynamic radius of the micelles based on PS-*b*-P4VP is ~ 12.00 nm. The hydrodynamic radii of micelles based on SMs gradually increases with increasing the volume fraction of P4VP(HOTPP), since HOTPP can induce more BCPs to be involved in the

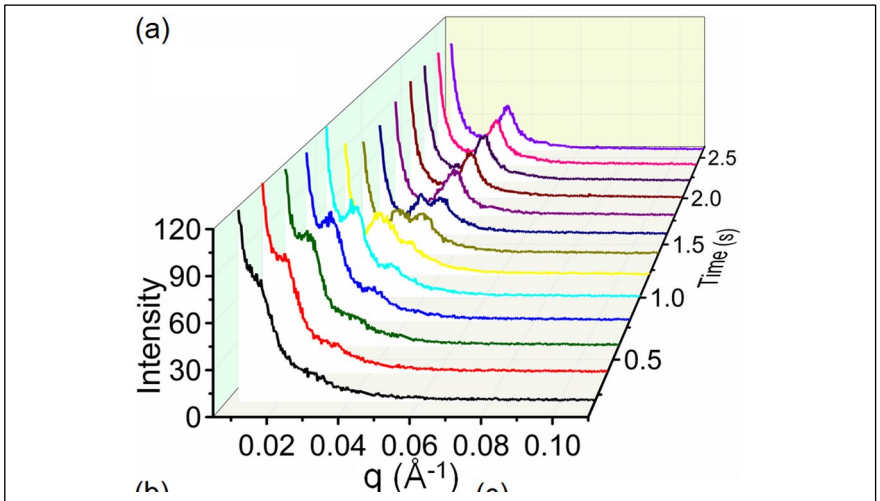

formation of [redacted] increases to ~ 40%, the size [redacted] microdomains remains cons[redacted]droxyl groups. Consequently, each HOTPP can hydrogen bond with four P4VP moieties which could lead to an increase in the size of the micelles. However, in the solid state, the size of the cylindrical microdomains remains essentially constant. For a higher concentrations of HOTPP, aggregates of HOTPP (Figure S1h/2i) are observed, indicating a saturation of the interactions of the PS-*b*-P4VP, with the excess HOTPP forming aggregates. As shown in Table 1 and Figure 1, the size of the microdomains observed is ~ 2 times smaller than the size of the micelles, due to solvent removal and the transformation from spherical micelles to cylindrical microdoains. In addition, THF, with a higher vapor pressure, evaporates more rapidly than toluene, allowing the core of the micelles to decrease initially, while the PS block remains solubilized. The reduction in the volume of the P4VP(HOTPP) also allows the HOTPPs to interact by π-stacking further promoting the formation of the cylindrical microdomains.

We investigated this transition by real-time *in situ* GISAXS (see Figure 3a/3b). Thin films were prepared using a mini slot-die coater mounted directly in the path of the incident x-ray beam.[32] Figure 3a shows the line cut of the GISAXS profiles based on SM7 thin film during the drying process. Figure 3a/3b shows the change in q_{max} of the SM7 thin film during drying. Initially, q_{max} is ~ 0.014 $Å^{-1}$ (d = ~ 44 nm), similar to the size of the micelles (~ 42 nm). With increasing time, i.e. solvent evaporation, the peak position changes from q_1 ~ 0.014 $Å^{-1}$ to 0.024 $Å^{-1}$decreases and then vanishes. After 1.0 second, a new interference at q_2 ~ 0.030 A^{-1} (d = ~ 21 nm) emerges and grows in intensity with increasing time. There is a relatively brief period of

time where both interferences are seen. Finally, after all the solvent has evaporated (~2.2 seconds), the scattering does not change. An AFM image of the dried film is shown in Figure 3c, where cylindrical microdomains oriented normal to the substrate are evident with a size of ~17 nm.

An SM7 thin film was prepared on an indium-tin oxide (ITO) glass substrate and an aluminum (Al) electrode (0.00126 cm^2) was evaporated onto the film surface to connect each microdomain in parallel. The areal density of microdomain (Figure S8) is ~ 2 x 10^{11} domains cm^{-2}, hence, each Al electrode contacts ~ 2.52 x 10^8 microdomains in parallel. The *I-V* characteristic of SM7 thin film was measured by Keithley 4200-SCS. At first, the current gradually increases with

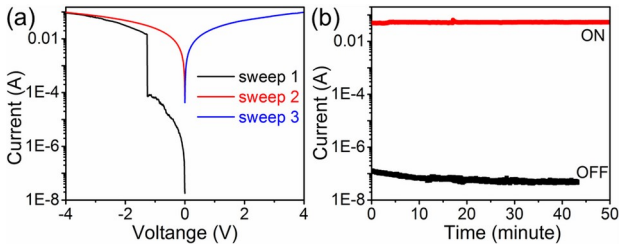

Figure 4. (a) The current-voltage characteristic of SM7 thin film. (b) Retention times at the ON and OFF states of the memory devices.

increasing voltage (Figure 4a). When the voltage increases to ~ -1.26 V, the current abruptly jumps from ~ 8.3 x 10^{-5} A to ~ 1.5 x 10^{-2} A. Finally, the current saturates at 0.10^{-1} A after the voltage was increased to -4 V. Assuming every microdomain was in contact with the two electrodes, the current carried by a single microdomain is ~ 4.0 nA. The transition from the OFF state to the ON state at -1.26 V can be used for a "write" process for a memory device.[33] The cell did not return to its original OFF state during a subsequent voltage sweep (sweep 2), even after applying a reverse voltage sweep (sweep 3). Consequently, the array shows a non-volatile write-

once-read many-times (WORM) characteristic. The stability of the ON state was measured. Figure 4b shows the retention time testing at different states. No noticeable current degradation was seen.

CONCLUSIONS

The hydrogen bonding between a functional small molecule, HOTPP, and the pyridine groups of the P4VP in a PS-*b*-P4VP BCP, was confirmed by the ^{1}H NMR and FTIR. SM7 was found to have the optimal balance with the highest volume fraction of P4VP(HOTPP) while maintaining film uniformity. A morphological transition from spherical micelles in solution to cylindrical microdomains oriented normal to the substrate during thin film drying was observed. The current of a single microdomain is estimated to ~ 4.0 nA through the *I-V* curve. Our finding shows promise of using SMs for further device applications. By introducing highly conductive materials into the microdomains, higher currents can be achieved, opening the possibility to decrease the size of the microdomains, and increasing the areal density of elements.

ASSOCIATED CONTENT

Supporting Information.

The following files are available free of charge. ^{1}H NMR, optical spectra, AFM images, GISAXS, GIWAXS, contact angles.

AUTHOR INFORMATION

Corresponding Author

*Email: russell@mail.pse.umass.edu

*E-mail: lujm@suda.edu.cn

The authors declare no competing financial interest.

ACKNOWLEDGMENT

This work was supported by the U.S. Department of Energy, Office of Science, Basic Energy Sciences under Contract No. DE-AC02-05-CH11231 within the Adaptive Interfacial Assemblies Towards Structuring Liquids program (KCTR16). This work was also supported by the National Natural Science Foundation of China 21776190 and 51803143. Pei-Yang Gu and Yufeng Jiang contributed equally.

ABBREVIATIONS

BCPs, block copolymers; ORM, organic resistance memory; ^{1}H NMR, proton nuclear magnetic resonance; FTIR, Fourier transform infrared; AFM, atomic force microscope; GISAXS, grazing incidence small-angle X-ray scattering.

REFERENCES

(1) Cheng, J. Y.; Mayes, A. M.; Ross, C. A., Nanostructure Engineering by Templated Self-Assembly of Block Copolymers. *Nat. Mater.* **2004**, *3*, 823-828.

(2) Jeong, S.-J.; Kim, J. Y.; Kim, B. H.; Moon, H.-S.; Kim, S. O., Directed Self-Assembly of Block Copolymers for Next Generation Nanolithography. *Mater. Today* **2013**, *16*, 468-476.

(3) Park, S.-M.; Liang, X.; Harteneck, B. D.; Pick, T. E.; Hiroshiba, N.; Wu, Y.; Helms, B. A.; Olynick, D. L., Sub-10 nm Nanofabrication *via* Nanoimprint Directed Self-Assembly of Block Copolymers. *ACS Nano* **2011**, *5*, 8523-8531.

(4) Rodriguez, A. T.; Li, X.; Wang, J.; Steen, W. A.; Fan, H., Facile Synthesis of Nanostructured Carbon through Self-Assembly between Block Copolymers and Carbohydrates. *Adv. Funct. Mater.* **2007**, *17*, 2710-2716.

(5) Hannon, A. F.; Ding, Y.; Bai, W.; Ross, C. A.; Alexander-Katz, A., Optimizing Topographical Templates for Directed Self-Assembly of Block Copolymers *via* Inverse Design Simulations. *Nano Lett.* **2014**, *14*, 318-325.

(6) Gao, Y.; Qiu, H.; Zhou, H.; Li, X.; Harniman, R.; Winnik, M. A.; Manners, I., Crystallization-Driven Solution Self-Assembly of Block Copolymers with a Photocleavable Junction. *J. Am. Chem, Soc.* **2015**, *137*, 2203-2206.

(7) Kim, J. Y.; Jin, H. M.; Jeong, S. J.; Chang, T.; Kim, B. H.; Cha, S. K.; Kim, J. S.; Shin, D. O.; Choi, J. Y.; Kim, J. H.; Yang, G. G.; Jeon, S.; Lee, Y. G.; Kim, K. M.; Shin, J.; Kim, S. O., Bimodal phase separated block copolymer/homopolymer blends self-assembly for hierarchical porous metal nanomesh electrodes. *Nanoscale* **2017**, *10*, 100-108.

(8) Mai, Y.; Eisenberg, A., Self-Assembly of Block Copolymers. *Chem. Soc. Rev.* **2012**, *41*, 5969-5685.

(9) Song, D. P.; Lin, Y.; Gai, Y.; Colella, N. S.; Li, C.; Liu, X. H.; Gido, S.; Watkins, J. J., Controlled Supramolecular Self-Assembly of Large Nanoparticles in Amphiphilic Brush Block Copolymers. *J. Am. Chem. Soc.* **2015**, *137*, 3771-3774.

(10) Crossland, E. J.; Cunha, P.; Scroggins, S.; Moratti, S.; Yurchenko, O.; Steiner, U.; Hillmyer, M. A.; Ludwigs, S., Soft-Etch Mesoporous Hole-Conducting Block Copolymer Templates. *ACS Nano* **2010**, *4*, 962-966.

(11) An, T. H.; La, Y.; Cho, A.; Jeong, M. G.; Shin, T. J.; Park, C.; Kim, K. T., Solution Self-Assembly of Block Copolymers Containing a Branched Hydrophilic Block into Inverse Bicontinuous Cubic Mesophases. *ACS Nano* **2015**, *9*, 3084-3096.

(12) Li, W.; Müller, M., Directed Self-Assembly of Block Copolymers by Chemical or Topographical Guiding Patterns: Optimizing Molecular Architecture, Thin-Film Properties, and Kinetics. *Prog. Polym. Sci.* **2016**, *54*, 47-75.

(13) Albert, J. N.; Epps III, T. H., Self-Assembly of Block Copolymer Thin films. *Mater. Today* **2010**, *13*, 24-33.

(14) Lee, B.; Park, I.; Yoon, J.; Park, S.; Kim, J.; Kim, K.-W.; Chang, T.; Ree, M., Structural Analysis of Block Copolymer Thin Films with Grazing Incidence Small-Angle X-Ray Scattering. *Macromolecules* **2005**, *38*, 4311-4323.

(15) O'Driscoll, S.; Demirel, G.; Farrell, R. A.; Fitzgerald, T. G.; O'Mahony, C.; Holmes, J. D.; Morris, M. A., The Morphology and Structure of PS-*b*-P4VP Block Copolymer Films by Solvent Annealing: Effect of the Solvent Parameter. *Polym. Adv. Technol.* **2011**, *22*, 915-923.

(16) Berezkin, A. V.; Papadakis, C. M.; Potemkin, I. I., Vertical Domain Orientation in Cylinder-Forming Diblock Copolymer Films upon Solvent Vapor Annealing. *Macromolecules* **2015**, *49*, 415-424.

(17) Posselt, D.; Zhang, J.; Smilgies, D.-M.; Berezkin, A. V.; Potemkin, I. I.; Papadakis, C. M., Restructuring in Block Copolymer Thin Films: In situ GISAXS Investigations during Solvent Vapor Annealing. *Prog. Polym. Sci.* **2017**, *66*, 80-115.

(18) Zhao, Y.; Thorkelsson, K.; Mastroianni, A. J.; Schilling, T.; Luther, J. M.; Rancatore, B. J.; Matsunaga, K.; Jinnai, H.; Wu, Y.; Poulsen, D.; Frechet, J. M.; Alivisatos, A. P.; Xu, T., Small-Molecule-Directed Nanoparticle Assembly towards Stimuli-Responsive Nanocomposites. *Nat. Mater.* **2009**, *8*, 979-985.

(19) Sidorenko, A.; Tokarev, I.; Minko, S.; Stamm, M., Ordered Reactive Nanomembranes/Nanotemplates from Thin Films of Block Copolymer Supramolecular Assembly. *J. Am. Chem. Soc.* **2003**, *125*, 12211-12216.

(20) Laiho, A.; Ras, R. H.; Valkama, S.; Ruokolainen, J.; Österbacka, R.; Ikkala, O., Control of Self-Assembly by Charge-Transfer Complexation between C_{60} Fullerene and Electron Donating Units of Block Copolymers. *Macromolecules* **2006**, *39*, 7648-7653.

(21) van Zoelen, W.; Polushkin, E.; Ten Brinke, G., Hierarchical Terrace Formation in PS-*b*-P4VP (PDP) Supramolecular Thin Films. *Macromolecules* **2008**, *41*, 8807-8814.

(22) Fujita, N.; Yamashita, T.; Asai, M.; Shinkai, S., Formation of [60]Fullerene Nanoclusters with Controlled Size and Morphology through the Aid of Supramolecular Rod-Coil Diblock Copolymers. *Angew. Chem. In. Ed.* **2005**, *44*, 1257-1261.

(23) Lee, K. H.; Bai, P.; Rancatore, B. J.; He, B.; Liu, Y.; Xu, T., Improved Hierarchical Ordering in Supramolecules via Symmetrically Bifunctionalized Organic Semiconductor. *Macromolecules* **2016**, *49*, 2639-2645.

(24) Rancatore, B. J.; Bai, P.; Xu, T., Organic Semiconductor-Based Supramolecular Nanocomposites. *Macromolecules* **2016**, *49*, 4155-4163.

(25) Tran, H.; Gopinadhan, M.; Majewski, P. W.; Shade, R.; Steffes, V.; Osuji, C. O.; Campos, L. M., Monoliths of Semiconducting Block Copolymers by Magnetic Alignment. *ACS Nano* **2013**, *7*, 5514-5521.

(26) Zhen, Y.; Inoue, K.; Wang, Z.; Kusamoto, T.; Nakabayashi, K.; Ohkoshi, S.-i.; Hu, W.; Guo, Y.; Harano, K.; Nakamura, E., Acid-Responsive Conductive Nanofiber of Tetrabenzoporphyrin Made by Solution Processing. *J. Am. Chem. Soc.* **2018**, *140*, 62-65.

(27) Li, Y.; Auras, F.; Lobermann, F.; Doblinger, M.; Schuster, J.; Peter, L.; Trauner, D.; Bein, T., A Photoactive Porphyrin-Based Periodic Mesoporous Organosilica Thin film. *J. Am. Chem. Soc.* **2013**, *135*, 18513-18519.

(28) Wu, S.; Bubeck, C., Macro- and Microphase Separation in Block Copolymer Supramolecular Assemblies Induced by Solvent Annealing. *Macromolecules* **2013**, *46*, 3512-3518.

(29) Rancatore, B. J.; Mauldin, C. E.; Tung, S.-H.; Wang, C.; Hexemer, A.; Strzalka, J.; Fréchet, J. M.; Xu, T., Nanostructured Organic Semiconductors *via* Directed Supramolecular Assembly. *ACS Nano* **2010**, *4*, 2721-2729.

(30) Kuila, B. K.; Gowd, E. B.; Stamm, M., Supramolecular Assembly of Poly(styrene)-*b*-poly(4-vinylpyridine) and 1-Pyrenebutyric Acid in Thin Film and Their Use for Nanofabrication. *Macromolecules* **2010**, *43*, 7713-7721.

(31) Chi, H. Y.; Hsu, H. W.; Tung, S. H.; Liu, C. L., Nonvolatile Organic Field-Effect Transistors Memory Devices using Supramolecular Block Copolymer/Functional Small Molecule Nanocomposite Electret. *ACS Appl. Mater. Interfaces* **2015**, *7*, 5663-5673.

(32) Park, S.; Wang, J.-Y.; Kim, B.; Chen, W.; Russell, T. P., Solvent-Induced Transition from Micelles in Solution to Cylindrical Microdomains in Diblock Copolymer Thin Films. *Macromolecules* **2007**, *40*, 9059-9063.

(33) Hu, Q.; Zhao, L.; Wu, J.; Gao, K.; Luo, D.; Jiang, Y.; Zhang, Z.; Zhu, C.; Schaible, E.; Hexemer, A.; Wang, C.; Liu, Y.; Zhang, W.; Gratzel, M.; Liu, F.; Russell, T. P.; Zhu, R.; Gong, Q., *In situ* Dynamic Observations of Perovskite Crystallisation and Microstructure Evolution Intermediated from $[PbI_6]^{4-}$ Cage Nanoparticles. *Nat. Commun.* **2017**, *8*, 15688-15696.

(34) Chen, Y.; Liu, G.; Wang, C.; Zhang, W.; Li, R.-W.; Wang, L., Polymer Memristor for Information Storage and Neuromorphic Applications. *Mater. Horiz.* **2014**, *1*, 489-506.

Graphic TOC Entry